https://doi.org/10.1016/j.ymssp.2021.108154

Ameliorated-Multiple Signal Classification (Am-MUSIC) for Damage Imaging Using A Sparse Sensor Network

Xiongbin Yang[a], Kai Wang[b], Pengyu Zhou[a], Lei Xu[a], Jinlong Liu[c], Peipei Sun[c], and Zhongqing Su[a,d,e*]

[a] Department of Mechanical Engineering
The Hong Kong Polytechnic University, Kowloon, Hong Kong SAR

[b] Interdisciplinary Division of Aeronautical and Aviation Engineering
The Hong Kong Polytechnic University, Kowloon, Hong Kong SAR

[c] Aero Engine Academy of China, Beijing, P.R. China

[d] The Hong Kong Polytechnic University Shenzhen Research Institute
Shenzhen 518057, P.R. China

[e] School of Astronautics, Northwestern Polytechnical University, Xi'an, 710072, P.R. China

submitted to ***Mechanical Systems and Signal Processing***

(first submitted on 7th January 2021; revised and resubmitted on 3rd June 2021)

* To whom correspondence should be addressed. Tel.: +852-2766-7818, Fax: +852-2365-4703, Email: Zhongqing.Su@polyu.edu.hk (Prof. Zhongqing SU, *PhD*)

Abstract

Multiple Signal Classification (MUSIC) – a directional scanning and searching algorithm, has gained its prominence in phased array-facilitated nondestructive evaluation. Nevertheless, prevailing MUSIC algorithms are largely bound up with the use of a dense linear array, which fail to access the full planar area of an inspected sample, leaving blind zones to which an array fails to scan, along with the incapability of differentiating multiple damage sites that are close one from another. To break above limitations, conventional MUSIC algorithm is ameliorated in this study, by manipulating the signal representation matrix at each pixel using the excitation signal series, instead of the scattered signal series, which enables the use of a sparse sensor network with arbitrarily positioned transducers. In the ameliorated MUSIC (Am-MUSIC), the orthogonal attributes between the signal subspace and noise subspace inherent in the signal representation matrix is quantified, in terms of which the Am-MUSIC yields a full spatial spectrum of the inspected sample, and damage, if any, can be visualized in the spectrum. Am-MUSIC is validated, in both simulation and experiment, by evaluating single and multiple sites of damage in plate-like waveguides with a sparse sensor network. Results verify that i) detectability of Am-MUSIC-driven damage imaging is not limited by damage quantity; ii) Am-MUSIC has full access to a sample, eliminating blind zones; and iii) the amelioration expands conventional MUSIC from phased array-facilitated nondestructive evaluation to health monitoring using built-in sparse sensor networks.

***Keywords*:** structural health monitoring; guided ultrasonic waves; multiple signal classification (MUSIC); phased array; sparse sensor network

1. Introduction

With the incentive to "*visualise*" hidden material defect or structural damage, continued effort has been made to projecting identified results, by means of proper imaging algorithms, in synthetic illustration, in which anomaly, if any, can be imaged intuitively [1]. Amongst various anomaly imaging approaches, those by virtue of guided ultrasonic waves (GUWs) have demonstrated eminent detectability, accuracy and precision [2-5], as represented by tomography-based imaging [6], delay-and-sum imaging [7], time-reversal focusing imaging [8], probability-based imaging [9], and array signal processing-based imaging [10-14], to name a few. Amongst them, the array signal processing-based imaging can be implemented in various modalities, including sparse reconstruction [10], minimum variance distortionless response method [11], subspace fitting [12], maximum-likelihood method [13], and Multiple Signal Classification (MUSIC) [14].

In particular, the MUSIC algorithm, with its theoretical framework shaped by Schmit [15] in 1981 for frequency estimation and radio direction finding, is a directional scanning and searching method to unbiasedly estimate signal features in terms of the orthogonal attributes between signal subspace and noise subspace. With a directional scanning ability, MUSIC has been extended to various application domains such as radar positioning [16], sonar [17], seismic exploration [18], biomedicine [19] and so forth. MUSIC has also proven effectiveness in GUW-based damage imaging. Representatively, Stepinski and Engholm [20] revamped a conventional MUSIC algorithm for estimating the *direction of arrival* (DOA) of incoming waves in plates with a uniform circular array. Yang *et al* [21, 22] employed the MUSIC algorithm to calculate the arrival times of impact-induced waves in conjunction with the use of wavelet transform, whereby to predict the location of an impact to a plate. Majority of MUSIC-driven damage evaluation lies in the *far-field hypothesis* that assumes a wave scatterer (e.g., damage) within the inspection region is sufficiently far from the phased array, so that the waves emanating from the scatterer can be considered as a plane wave when they arrive at the array, as illustrated schematically in **Fig. 1(a)**.

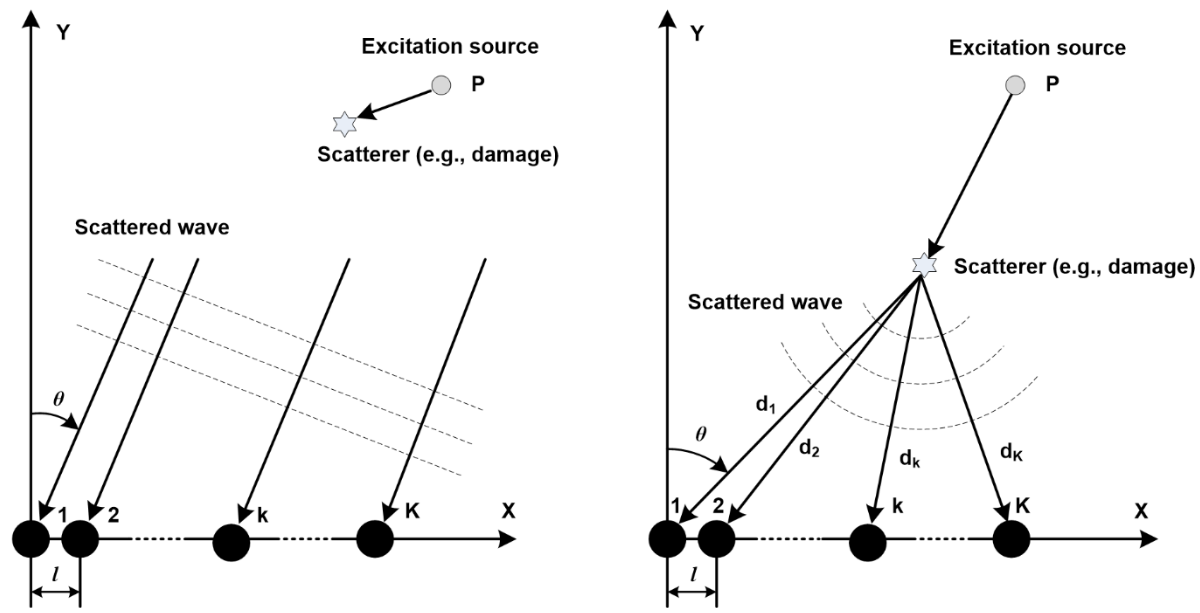

(a) (b)

Fig. 1. Use of phased array for evaluation of damage in a planar inspection region [23]: (a) far-field scenario; and (b) near-field scenario (d_k : the distance from the wave source through the damage then to the k_{th} array element).

Despite demonstrated effectiveness in numerous applications, the *far-field hypothesis* is often questioned in practical implementation, as the damage location is unknown *a priori*, and the wavefront scattered by the damage is naturally cylindrical rather than planar, provided the damage is in the near-field – the scenario in **Fig. 1(b)**. In recognition of such deficiency that prevailing MUSIC algorithms inherently has, enhancement has been made to improve conventional MUSIC-driven damage evaluation. Zhong *et al* [23, 24] developed a revamped MUSIC algorithm based on the Taylor expansion theory, applicable to detecting near-field damage in a composite oil tank. Extending this study, Yuan *et al* [25] took into account the anisotropy of composite structures and proposed a single-frequency component-based MUSIC algorithm able to improve the precision of locating a near-field impact site in composites. Zuo *et al* [26] calculated the cross-correlation function for the scattered signals received by a damage scattering model and the residual signals received in experiment, and applied the two-dimensional (2-D) MUSIC algorithm to identify damage in plate-like structures. Bao *et al* [27] combined the transmitter beamforming and weighted image fusion to enhance the conventional MUSIC, endowing it with the capability of localizing near-field corrosion in aluminum plates. Bao *et al* [28] further proposed a compensated MUSIC algorithm by considering the effect of both the localization error caused by structural anisotropy and the sensor position error, showing improved detection accuracy.

Notwithstanding the forgoing, the prevailing MUSIC-based damage imaging approaches in general present the following limitations:

i) *use of linear phased arrays*: the MUSIC algorithm, as an eigen-structure mathematic approach, is not inherently restricted to the use of linear arrays. When used for damage identification, a linear array that features a dense configuration of transmitter elements is usually adopted, and the element pitch (l) shall be uniform and small enough, ideally satisfying $l \leq \lambda / 2$ (λ : the wavelength of the wave generated by the array [29]), to facilitate construction of the signal representation matrix with the scattered signal series. In general, the conventional MUSIC algorithms do not sustain the use of a sparse sensor network with individual sensors at arbitrary locations;

ii) *existence of blind zone*: the beamforming capacity of the algorithm degrades when the scanning angle is close to 0° or 180°. In most circumstances, those regions, where the scanning angles are in the range of [0, 30] or [150, 180], are deemed blind zones [30], in which damage, if any, may be overridden;

iii) *ambiguous results due to mirror effect*: the identified damage using a MUSIC algorithm might be a mirrored dummy of the true damage which is located symmetrically with regard to the array surface [31]; and

iv) *obscure multiple damage sites:* when MUSIC is used for imaging multiple damage sites, the number of scatterers shall be predicted beforehand. To this end, a threshold is selected, and the eigenvalues of the covariance matrix of the received signals that are larger than this threshold shall be counted as the number of the scatterers. However, selection of the threshold is a highly subjective manner at the discretion of individuals, and it is prone to contamination of measurement noise [32]. This results in inferior imaging resolution and makes it challenging to differentiate multiple damage sites that are close one from another.

Aimed at surmounting the above limitations that prevailing MUSIC-based damage imaging approaches may encounter, an ameliorated MUSIC (Am-MUSIC) algorithm is developed by manipulating the signal representation matrix at each image pixel using the excitation signal series instead of the scattered signal series. Thanks to that, Am-MUSIC algorithm does not necessarily entail the use of a linear phased array, and instead it is compatible with a sparse sensor network in which individual transducers can be positioned arbitrarily. At each image pixel, the orthogonal attributes between the signal subspace and noise subspace inherent in signal representation matrix is quantified, in terms of which Am-MUSIC yields a full spatial spectrum of the inspected sample, to visualize damage, regardless of its quantity in the sample. Both simulation and experiment are performed to validate the Am-MUSIC algorithm, by evaluating single and multiple sites of damage in plate-like waveguides with a sparse sensor network comprising only a handful of miniaturized lead zirconate titanate (PZT) wafers.

The rest of this paper is organized as follows. The conventional MUSIC-driven damage imaging, based on the near-field hypothesis, is briefed in Section 2, on which basis the Am-MUSIC algorithm is developed, with key amelioration detailed in Section 3. Numerical verification of Am-MUSIC is illustrated in Section 4, followed with experimental validation in Section 5.

2. Near-Field MUSIC Algorithm

GUWs guided by a plate-like waveguide, a.k.a. *Lamb waves*, are of a multimodal and dispersive nature. At a given frequency, Lamb waves feature a multitude of wave modes which can be classified as the symmetric and antisymmetric modes. We consider a pure, monochromatic Lamb wave mode in the waveform of a toneburst, as the excitation signal $s(t)$. $s(t)$ is defined in a complex domain as

$$s(t) = u(t)\exp^{i\omega_0 t}, \tag{1}$$

where $u(t)$ denotes a window function to regulate the toneburst, t the time, i the imaginary unit, and ω_0 the central frequency of the toneburst. With the attenuation in magnitude as wave propagation in consideration, the Lamb wave, $R(\omega)$, after travelling the distance d can be represented, in the frequency domain, as

$$R(\omega) = \frac{d_0}{\sqrt{d}} S(\omega)\exp^{-ikd}. \tag{2}$$

In the above, d_0 signifies an initial distance with regard to which the wave attenuation is calibrated; $S(\omega)$ is the corresponding Fourier representation of $s(t)$; $k = \frac{\omega_0}{c}$, where k denotes the wavenumber and c represents the propagation velocity of the considered monochromatic Lamb wave mode.

Substituting Eqs. (1) into (2), the Lamb wave $r(t)$ when it arrives at the distance d can be yielded, in the time domain, as

$$r(t) = \frac{d_0}{\sqrt{d}} F^{-1}\left\{ s(\omega)\exp^{-i\frac{w_0}{c}d} \right\} = \frac{d_0}{\sqrt{d}} s(t-\frac{d}{c}) = \frac{d_0}{\sqrt{d}} u(t-\frac{d}{c})\exp^{i\omega_0 (t-\frac{d}{c})}, \tag{3}$$

where $r(t)$ is the inverse Fourier transform of $R(\omega)$ and F^{-1} is the inverse Fourier transform.

For an intact waveguide, the captured wave signal, denoted with $r^{\text{measured-intact}}(t)$, is the direct arrival wave $r^{\text{direct}}(t)$, boundary-reflection wave $r^{\text{boundary-reflection}}(t)$ with incoherent noise $w^{\text{measured-intact}}(t)$, as

$$r^{\text{measured-intact}}(t) = r^{\text{direct}}(t) + r^{\text{boundary-reflection}}(t) + w^{\text{measured-intact}}(t), \tag{4}$$

where $r^{\text{direct}}(t)$ is the arrival wave propagating along the path from the wave source to the wave receiver. Provided damage is present at an unknown location in the waveguide, the damage can be modeled as a secondary wave source to scatter the incoming Lamb waves. Ignoring mode conversion that is fairly weak in magnitude, the measured signal $r^{\text{measured-damage}}(t)$ comprises the direct arrival wave $r^{\text{direct}}(t)$, boundary-reflection wave $r^{\text{boundary-reflection}}(t)$, additional scattered wave from the damage $r^{\text{scattered}}(t)$, and the incoherent noise $w^{\text{measured-damage}}(t)$, as

$$r^{\text{measured-damage}}(t) = r^{\text{direct}}(t) + r^{\text{boundary-reflection}}(t) + r^{\text{scattered}}(t) + w^{\text{measured-damage}}(t), \tag{5}$$

where $r^{\text{scattered}}(t)$ is the arrival wave propagating along a scattered path (namely, the path from the wave source to the damage and then to the wave receiver). Suppose that the direct waves and boundary-reflection waves are the same at $r^{\text{measured-intact}}(t)$ and $r^{\text{measured-damage}}(t)$, $r^{\text{scattered}}(t)$ which carries information pertaining to the damage location can be obtained through benchmarking reference signals obtained from the intact status, as

$$r^{\text{measured-damage}}(t) - r^{\text{measured-intact}}(t) = r^{\text{scattered}}(t) + w(t) = r^{\text{residual}}(t), \tag{6}$$

where $w(t)$ is the difference between the two noise terms $w^{\text{measured-intact}}(t)$ and $w^{\text{measured-damage}}(t)$ in the intact and current statuses. Here, for convenience of discussion, the terms of $r^{\text{scattered}}(t) + w(t)$ is referred to as the *residual signal*.

With the near-field assumption, as schematically illustrated in **Fig. 1(b)**, Lamb wave is excited at a foreknown position *P*, scattered by the damage, and then received by a linear sensor array that consisting of *K* transducing elements with a uniform element spacing *l*. According to Eq. (3), the scattered signal received by the first array element, $r_1^{\text{scattered}}(t)$, is

$$r_1^{\text{scattered}}(t) = \frac{d_0}{\sqrt{d_1}} s(t - \frac{d_1}{c}) = \frac{d_0}{\sqrt{d_1}} u(t - \frac{d_1}{c}) \exp^{i\omega_0 (t - \frac{d_1}{c})}, \tag{7}$$

where d_1 signifies the distance from the wave source through the damage then to the first array element. Let $\tau_k = \frac{d_1 - d_k}{c}$ (*i.e.*, the time delay between two arrival signals captured by the first and the k^{th} (k=1, 2, …, K) element in the array), and then the scattered wave signal received by the k^{th} element, $r_k^{\text{scattered}}(t)$, can be expressed as

$$r_k^{\text{scattered}}(t) = \frac{d_0}{\sqrt{d_k}} s(t - \frac{d_k}{c}) = \frac{d_0}{\sqrt{d_k}} u(t - \frac{d_k}{c}) \exp^{i\omega_0 (t - \frac{d_k}{c})} = \frac{d_0}{\sqrt{d_k}} u(t - \frac{d_1}{c} + \tau_k) \exp^{i\omega_0 (t - \frac{d_1}{c} + \tau_k)} . \quad \left(k = 1, 2, \ldots, K\right) \tag{8}$$

With the assumption that the array element spacing l is sufficiently small (namely, $l \le \lambda / 2$, where λ is the wavelength of wave signal), $r_k^{\text{scattered}}(t)$ can be obtained based on the first element scattered signal $r_1^{\text{scattered}}(t)$ (defined in Eq. (7)) as

$$\begin{aligned} r_k^{\text{scattered}}(t) &= \frac{d_0}{\sqrt{d_k}} u(t - \frac{d_1}{c} + \tau_k) \exp^{i\omega_0 (t - \frac{d_1}{c} + \tau_k)} \\ &\approx \frac{d_0}{\sqrt{d_k}} u(t - \frac{d_1}{c}) \exp^{i\omega_0 (t - \frac{d_1}{c} + \tau_k)} \\ &= \sqrt{\frac{d_1}{d_k}} r_1^{\text{scattered}}(t) \exp^{i\omega_0 \tau_k} . \end{aligned} \tag{9}$$

According to the cosine theorem [33] and second-order Taylor expansion [34], τ_k can be re-written as

$$\begin{aligned} \tau_k &= \frac{d_1 - d_k}{c} = \frac{d_1 - \sqrt{d_1^{\,2} + (k-1)^2 l^2 - 2 d_1 (k-1) l \cos(90^{\circ} - \theta)}}{c} \\ &= \frac{-l \sin\theta}{c}(k-1) + (\frac{-l^2}{c d_1} \cos\theta^2)(k-1)^2 + O(\frac{l^2}{d_1^{\,2}}) , \end{aligned} \tag{10}$$

where $O(\frac{l^2}{d_1^{\,2}})$ denotes those terms, the order of which is greater than or equal to $\frac{l^2}{d_1^{\,2}}$. Using the second-order Taylor series approximation, the scattered wave signal received by the k^{th} element retreats to

$$r_k^{\text{scattered}}(t) = \sqrt{\frac{d_1}{d_k}} r_1^{\text{scattered}}(t) \exp^{i\omega_0 \tau_k} = \sqrt{\frac{d_1}{d_k}} r_1^{\text{scattered}}(t) \exp^{i\omega_0 (\frac{-l \sin\theta}{c}(k-1) + (\frac{-l^2}{c d_1} \cos\theta^2)(k-1)^2)} . \tag{11}$$

Letting $b_k(d, \theta) = \sqrt{\frac{d_1}{d_k}} \exp^{i\omega_0 (\frac{-l \sin\theta}{c}(k-1) + (\frac{-l^2}{c d_1} \cos\theta^2)(k-1)^2)}$, as the array steering factor for the k^{th} scattered signal, and recalling the noise term in Eq. (6), the k^{th} residual signal, $r_k^{\text{residual}}(t)$, can be expressed as

$$r_k^{\text{residual}}(t) = b_k(d, \theta) r_1^{\text{scattered}}(t) + w_k(t) . \tag{12}$$

For the linear array with K elements, the residual signal vector $\mathbf{R}^{\text{residual}}(t)$ can thus be obtained and expressed in a signal representation matrix, which reads

$$\mathbf{R}^{\text{residual}}(t) = \mathbf{B}(d,\theta) r_1^{\text{scattered}}(t) + \mathbf{W}(t), \tag{13}$$

where

$$\mathbf{R}^{\text{residual}}(t) = [r_1^{\text{residual}}(t), \cdots, r_k^{\text{residual}}(t), \cdots, r_K^{\text{residual}}(t)]^T,$$

$$\mathbf{B}(d,\theta) = [b_1(d,\theta), \cdots, b_k(d,\theta), \cdots, b_K(d,\theta)]^T = \begin{bmatrix} 1 \\ \vdots \\ \sqrt{\dfrac{d_1}{d_k}} \exp^{i\omega_0 (\frac{-l\sin\theta}{c}(k-1) + (\frac{-l^2}{cd_1}\cos\theta^2)(k-1)^2)} \\ \vdots \\ \sqrt{\dfrac{d_1}{d_K}} \exp^{i\omega_0 (\frac{-l\sin\theta}{c}(K-1) + (\frac{-l^2}{cd_1}\cos\theta^2)(K-1)^2)} \end{bmatrix},$$

$$\mathbf{W}(t) = [w_1(t), \cdots, w_k(t), \cdots, w_K(t)]^T.$$

Prevailing MUSIC-based damage imaging approaches have been developed by virtue of the signal representation matrix as defined in Eq. (13). They, in general, present the following limitations during practical implementation, as preliminarily commented in the preceding section:

i) In Eq. (9), the operation of approximation, $u(t - \frac{d_1}{c} + \tau_k) \approx u(t - \frac{d_1}{c})$, lies in the premise that τ_k is negligibly small. To accommodate such a pre-requisite, the element spacing in the phased array must be sufficiently small ($l \leq \lambda / 2$), leading to a dense configuration of the transducing elements; and

ii) In Eq. (11), the steering vector is approximated using the second-order Taylor approximation, and the range error introduced by such approximation is remarkable when the damage is close to the array. For a range that is smaller than twice the array length (i.e., the length from the first element to the k^{th} element), such error could be 10% or above due to such approximation [35]. In addition, the steering vectors at the scanning angles θ and $180^{\circ} - \theta$ have the same value in Eq. (11), resulting in ambiguous results due to mirror effect.

3. Am-MUSIC with A Sparse Sensor Network

Aimed at circumventing the above key limitations that conventional MUSIC-based damage imaging possesses, the original MUSIC algorithm is revamped. Different from the use of a linear phased array, we allow a sparse sensor network with individual transducers that are randomly positioned. Without loss of generality, consider a sparse sensor network comprising *Q* PZT wafers (labelled as PZT-*1*, PZT-*2*, …, PZT-*j*, …, PZT-*Q*), as shown in **Fig. 2**. Positioned at an arbitrary location within the inspection region, each PZT wafer acts as either a wave transmitter or a wave receiver, leading to $M = Q(Q-1)/2$ transmitter–receiver pairs in the sensor network. Provided damage exists at pixel (x, y) within the inspection area, the propagation distance, d_{mxy}, for a Lamb wave, which is generated by the i^{th} transmitter at (x_i, y_i), scattered by damage at (x, y) and then propagates to the j^{th} receiver at (x_j, y_j), is

$$d_{mxy} = \sqrt{(x-x_i)^2 + (y-y_i)^2} + \sqrt{(x-x_j)^2 + (y-y_j)^2} = c \cdot t_{mxy}, \tag{14}$$

and t_{mxy} is the time for the wave traveling along the scattered path.

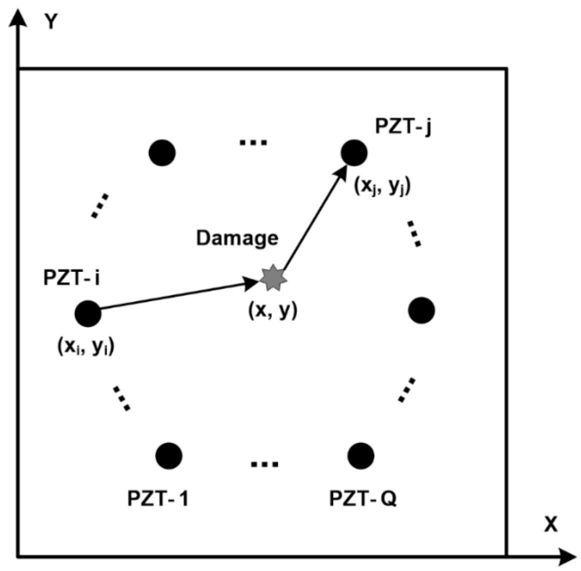

Fig. 2. A plate waveguide with a sparse sensor network of *Q* PZT wafers.

Therefore, the scattered signal received by the m^{th} transmitter–receiver pair, $r_m^{\text{scattered}}(t)$, can be written according to Eq. (3) as

$$r_m^{\text{scattered}}(t) = \frac{d_0}{\sqrt{d_{mxy}}} s\left(t - \frac{d_{mxy}}{c}\right) \qquad (m = 1, 2, \ldots, M). \tag{15}$$

Equation (15) argues that for *M* transmitter–receiver pairs rendered by the sensor network, different scattering paths feature different degrees of time delay. A time shift, t_{mxy}, is then applied to the m^{th} scattered signal $r_m^{\text{scattered}}(t)$ in Eq. (15), as

$$r_m^{\text{scattered}}(t+t_{mxy}) = \frac{d_0}{\sqrt{d_{mxy}}} s(t - \frac{d_{mxy}}{c} + t_{mxy}) = \frac{d_0}{\sqrt{d_{mxy}}} s(t) . \tag{16}$$

Letting $a_{mxy} = \dfrac{d_0}{\sqrt{d_{mxy}}}$ (a_{mxy} is referred to as the *array steering factor* for the m^{th} scattered signal in what follows), Eq. (16) can be rewritten as

$$r_m^{\text{scattered}}(t+t_{mxy}) = a_{mxy} s(t) . \tag{17}$$

With the noise term ($w(t)$ in Eq. (6)) in consideration, the residual signal vector for a total of M received signals which are respectively scattered by the damage at pixel (x, y), $\mathbf{R}_{xy}^{\text{residual}}(t)$, can be expressed as the signal representation matrix

$$\mathbf{R}_{xy}^{\text{residual}}(t) = \mathbf{A}_{xy} s(t) + \mathbf{W}(t) , \tag{18}$$

where

$$\mathbf{R}_{xy}^{\text{residual}}(t) = [r_1^{\text{residual}}(t+t_{1xy}), \cdots, r_m^{\text{residual}}(t+t_{mxy}), \cdots, r_M^{\text{residual}}(t+t_{Mxy})]^T ,$$

$$\mathbf{A}_{xy} = [a_{1xy}, \cdots, a_{mxy}, \cdots, a_{Mxy}]^T ,$$

$$\mathbf{W}(t) = [w_1(t+t_{1xy}), \cdots, w_m(t+t_{mxy}), \cdots, w_M(t+t_{Mxy})]^T .$$

Equation (18) implies that after compensating for the time delay to each residual signal, the residual signal vector can be defined using the excitation signal series, instead of using the scattered signal series as a conventional MUSIC algorithm does (Eq. (13)). It is such a merit of the ameliorated MUSIC (Am-MUSIC) algorithm that enables the use of a sparse sensor network with arbitrarily positioned transducers.

Recalling the MUSIC algorithm, the covariance matrix $\mathbf{C}$ of the residual signal vector at pixel (x, y) within the inspection region yields as

$$\begin{aligned} \mathbf{C} &= E[\mathbf{R}_{xy}^{\text{residual}}(t)\mathbf{R}_{xy}^{\text{residual}}(t)^H] \\ &= \mathbf{A}_{xy} E\left[s(t)\cdot s(t)^H\right]\mathbf{A}_{xy}{}^H + \mathbf{A}_{xy} E\left[s(t)\cdot \mathbf{W}(t)^H\right] + E\left[\mathbf{W}(t)\cdot s(t)^H\right]\mathbf{A}_{xy}{}^H + E\left[\mathbf{W}(t)\cdot \mathbf{W}(t)^H\right], \end{aligned} \tag{19}$$

where $E[\ ]$ denotes covariance computation, and superscript H represents the complex conjugate transpose.

As the source signal and noise signal are uncorrelated and mutually independent, the covariance matrix $\mathbf{C}$ can be simplified as

$$\mathbf{C} = \mathbf{A}_{xy}\mathbf{R}_s\mathbf{A}_{xy}{}^H + \sigma^2\mathbf{I} , \tag{20}$$

where $\mathbf{R}_s = E\left[s(t)\, s(t)^H \right]$, and it signifies the covariance matrix of the source signal. σ^2 is noise power and $\mathbf{I}$ the covariance matrix of the noise signal. The covariance matrix $\mathbf{C}$ can be decomposed into two parts: namely a signal-related part and a noise-related part, as

$$\mathbf{C} = \mathbf{U}\mathbf{\Sigma}\mathbf{U}^H = \mathbf{U}_S\mathbf{\Sigma}\mathbf{U}_S{}^H + \mathbf{U}_N\mathbf{\Sigma}\mathbf{U}_N{}^H, \quad (21)$$

where $\mathbf{U} = [\mu_1, \mu_2, \cdots, \mu_M]$, and the columns of $\mathbf{U}$ are the singular vectors; $\mathbf{\Sigma}$ is a diagonal matrix with singular values arranged in a descending order of magnitudes. Considering that $\mathbf{A}_{xy}$ is the steering vector at pixel (x, y) with the dimension of $M \times 1$ and $\mathbf{A}_{xy}\mathbf{R}_s\mathbf{A}_{xy}{}^H$ in Eq. (20) is decomposed as $\mathbf{U}_S\mathbf{\Sigma}\mathbf{U}_S{}^H$ in Eq. (21), $\mathbf{U}_S = [\mu_1]$ denoting the signal subspace spanned by the eigenvectors corresponding to the first largest eigenvalue; and $\mathbf{U}_N = [\mu_2, \mu_3, \cdots, \mu_M]$, representing the noise subspace spanned by the eigenvectors corresponding to the remaining M - 1 eigenvalues.

Based on Eqs. (20) and (21), the following expression can be obtained after multiplying covariance matrix $\mathbf{C}$ with the noise subspace $\mathbf{U}_N$

$$\mathbf{A}_{xy}\mathbf{R}_s\mathbf{A}_{xy}{}^H\mathbf{U}_N = \mathbf{0}. \quad (22)$$

As $\mathbf{R}_s$ is a full rank matrix, Eq. (22) is further simplified as

$$\mathbf{A}_{xy}{}^H\mathbf{U}_N = \mathbf{0}. \quad (23)$$

Equation (23) argues that the steering vector $\mathbf{A}_{xy}$ at the position of damage is orthogonal with the noise subspace $\mathbf{U}_N$. This characteristic makes it possible for the Am-MUSIC to calculate the steering vector at each pixel across the entire inspection region and calibrate the degree of orthogonality between the steering vector and the noise subspace with the squared norm of vector $\mathbf{A}_{xy}{}^H\mathbf{U}_N$ as

$$\beta^2 = \left\| \mathbf{A}_{xy}{}^H\mathbf{U}_N \right\|^2 = \mathbf{A}_{xy}{}^H(\mathbf{U}_N\mathbf{U}_N{}^H)\mathbf{A}_{xy}\ . \quad (24)$$

Taking a reciprocal of the squared norm expression creates a peak in the spatial spectrum that corresponds to the damage location. Am-MUSIC algorithm defines the pixel value ($P_{\text{Am-MUSIC}}(x, y)$) within the inspection region as

$$P_{\text{Am-MUSIC}}(x, y) = \frac{1}{\mathbf{A}_{xy}{}^H(\mathbf{U}_N\mathbf{U}_N{}^H)\mathbf{A}_{xy}}. \quad (25)$$

Equation (24) yields a full spatial spectrum for the inspection region, in which $P_{\text{Am-MUSIC}}(x, y)$ culminates at the damage location.

In summary, the complete procedure of the proposed Am-MUSIC algorithm is flowcharted in a nutshell in **Fig. 3**. Notably, the Am-MUSIC algorithm calculates the signal representation matrix at each pixel throughout the entire inspection region, and it is therefore the number of scatterers (i.e., the number of multiple damage sites) is no longer required, in contrast to a conventional MUSIC algorithm in which the number of scatterers shall be predicted beforehand at a subjective discretion of individuals. It is also noteworthy that the computational cost of Am-MUSIC does not intend to increase compared with conventional MUSIC algorithms, regardless of the fact that the calculation is performed at every signal pixel – that is because the signal representation matrix can be formed cost-effectively and the steering factor in Eq. (18) can be calculated efficiently compared with that of conventional MUSIC algorithm in Eq. (13). In addition, it is such a merit of the Am-MUSIC algorithm that makes it possible to gauge the local region of interest (RoI) only – the vicinity in the sample where damage may exist, rather than scanning the entire sample. Such a merit remarkably lowers the computational cost and unburdens computing hardware when the inspection region has of large dimensions.

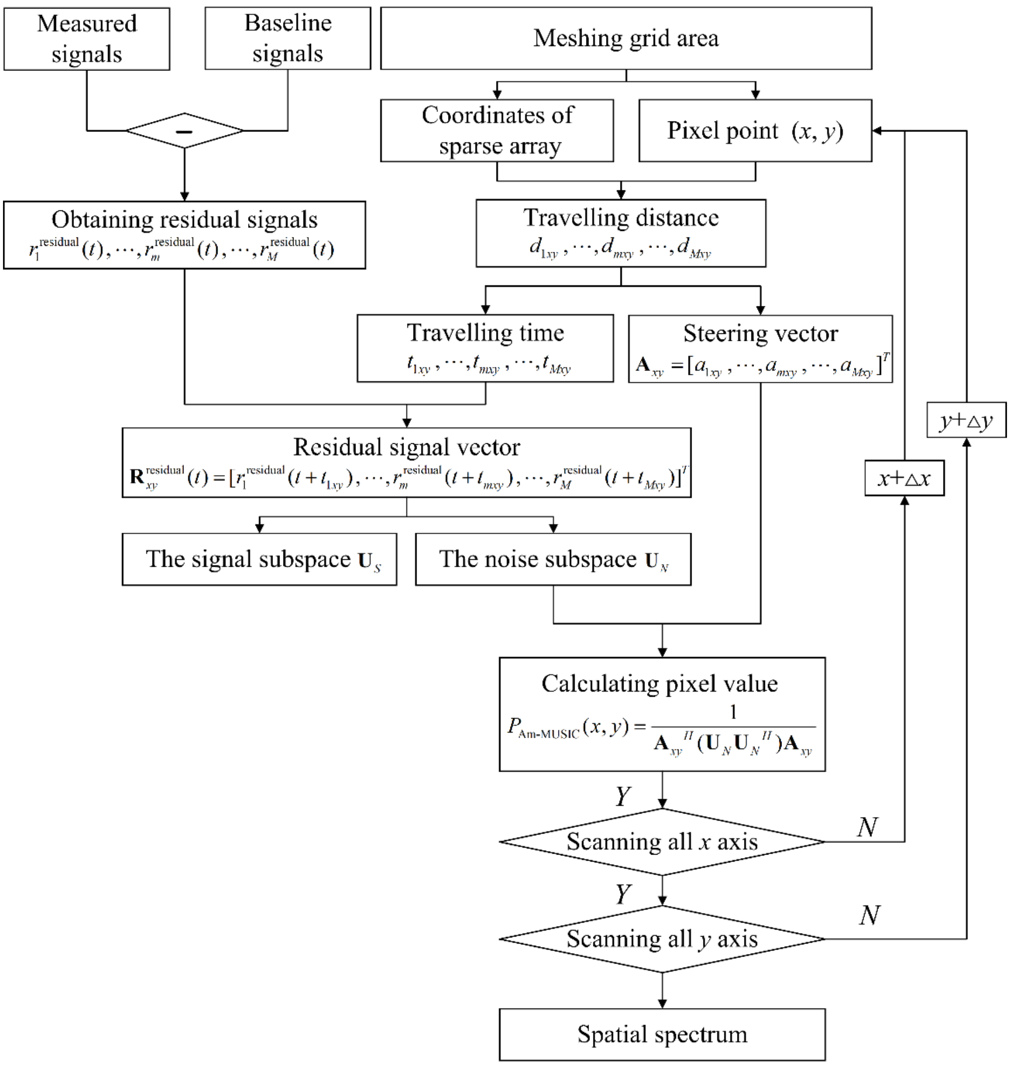

Fig. 3. Key steps of Am-MUSIC algorithm.

4. Numerical Validation

To validate the developed Am-MUSIC algorithm for damage imaging, numerical simulation is implemented first. Consider a homogeneous, isotropic plate-like waveguide (density: ρ=2,700 kg/m^3; Young modulus: E=71 GPa; Poisson's ratio ν=0.33), measuring 500 mm × 500 mm × 2 mm. Atop the waveguide there is a sparse sensor network with only six PZT wafers, as illustrated in **Fig. 4(a)**. Each PZT wafer functions as either a wave transmitter or a wave receiver, leading to 15 transmitter-receiver pairs in the sensor network. For comparison against conventional MUSIC, another seven PZT wafers are arranged in a linear array as sensors, in **Fig. 4(b)**, along with an additional PZT wafer as wave actuator placed at the position (250 mm, 400 mm). In all cases, a 3-cycle Hanning window tone burst with central frequency 200 kHz signal is selected as excitation signal to obtain S_0 wave mode, considering wave sensitivity and excitability. A total duration of 150 μs time length is analyzed for all numerical cases.

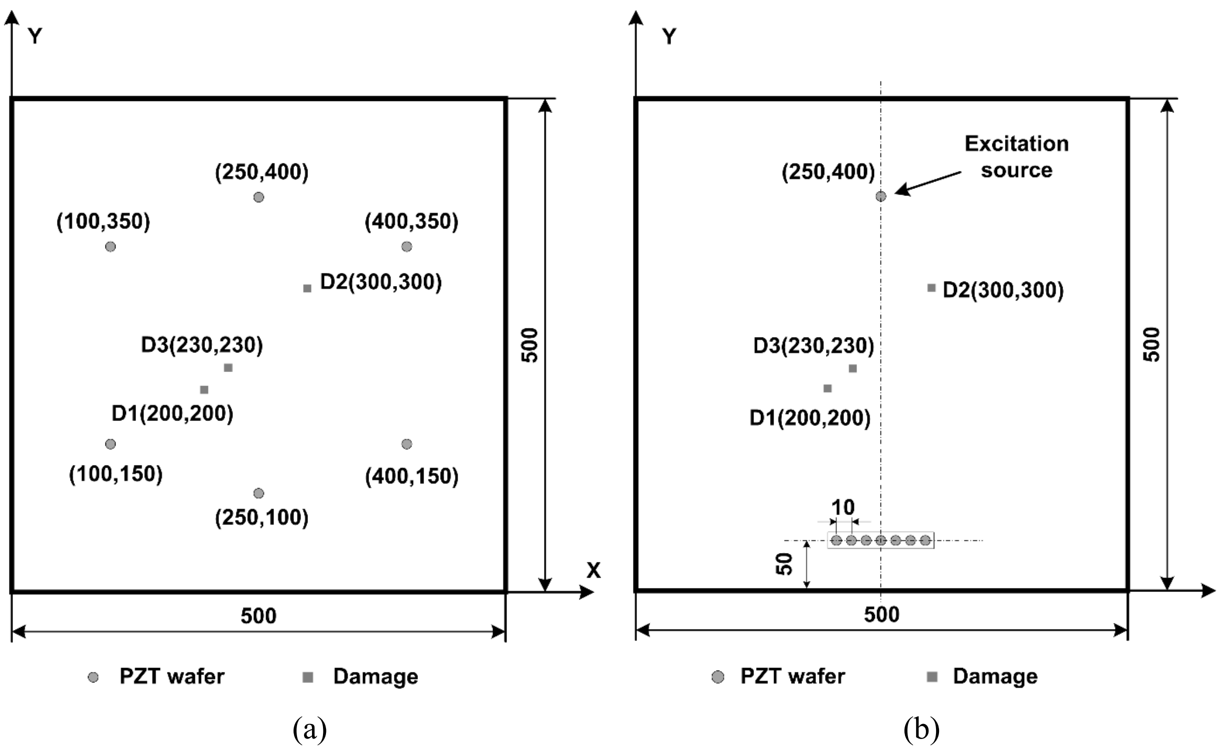

Fig. 4. Schematics of the plate waveguide in simulation (all dimensions in mm): (a) with a sparse sensor network for Am-MUSIC algorithm; and (b) with a linear array for conventional MUSIC algorithm.

Damage in the simulation is introduced to the waveguide by enforcing the material local stiffness to be zero. Three damage sites, labeled as D1-D3, are simulated in the waveguide, with respective positions highlighted in **Fig. 4** and summarized in **Table 1**. With these damage sites, three damage cases (C-I – C-III) are created by including different damage sites, **Table 2**.

Table 1 Three damage sites in simulation

Damage site	Position	
	x [mm]	y [mm]
D1	200	200
D2	300	300
D3	230	230

Table 2 Three damage cases in simulation

Damage case	Damage site included
C-I	D1
C-II	D1, D2
C-III	D1, D3

Figure 5(a) displays the spatial spectrum obtained using the Am-MUSIC algorithm, for C-I – the case with only a single damage site (D1), accurately pinpointing the damage location (200 mm, 200 mm). For comparison, the image constructed using the conventional MUSIC algorithm is shown in **Fig. 5(b)**, indicating the damage location at (197 mm, 208 mm), which represents an error of (3 mm, 8 mm), in addition to an elongation artifact along the damage direction – a common deficiency for conventional MUSIC algorithms as illustrated elsewhere [21-25, 36]. The degree of such artifact depends on the signal-to-noise ratio and the point-spread function of the phased array at the location of the scatterer [37].

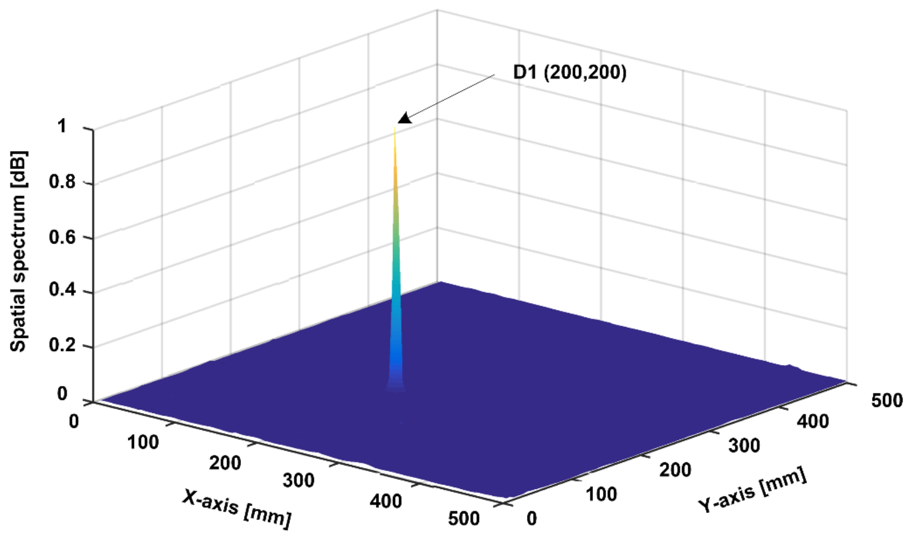

(a)

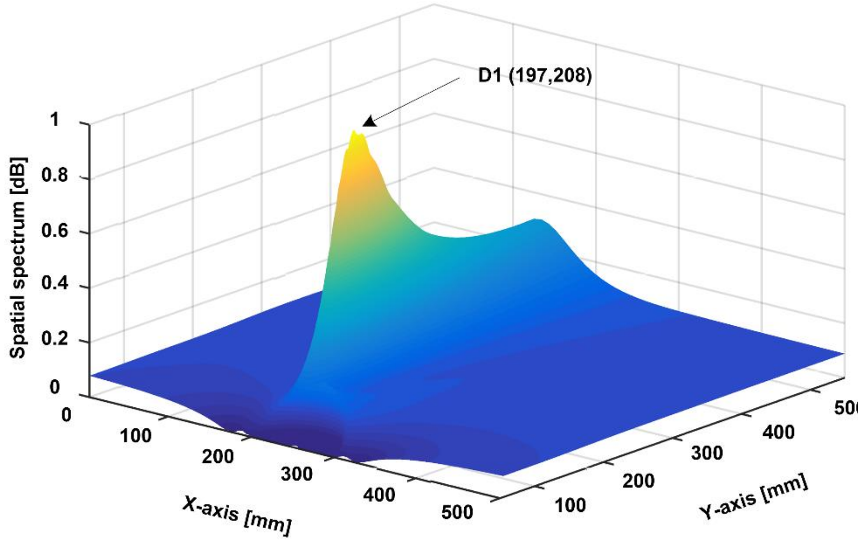

(b)

Fig. 5. Spatial spectra for C-I obtained by (a) Am-MUSIC algorithm; and (b) conventional MUSIC algorithm.

Figure 6(a) shows the spectrum for C-II obtained using the Am-MUSIC. Again, the identified results are observed to coincide exactly with actual damage sites, contrasting the spatial spectrum obtained using the conventional MUSIC algorithm in **Fig. 6(b)**, in which two damage sites are predicted with notable error. In addition, the peak at D1 location is much stronger than that at D2 as noted in **Fig. 6(b)**, contradicting the fact that D1 and D2 actually have the same degree of severity.

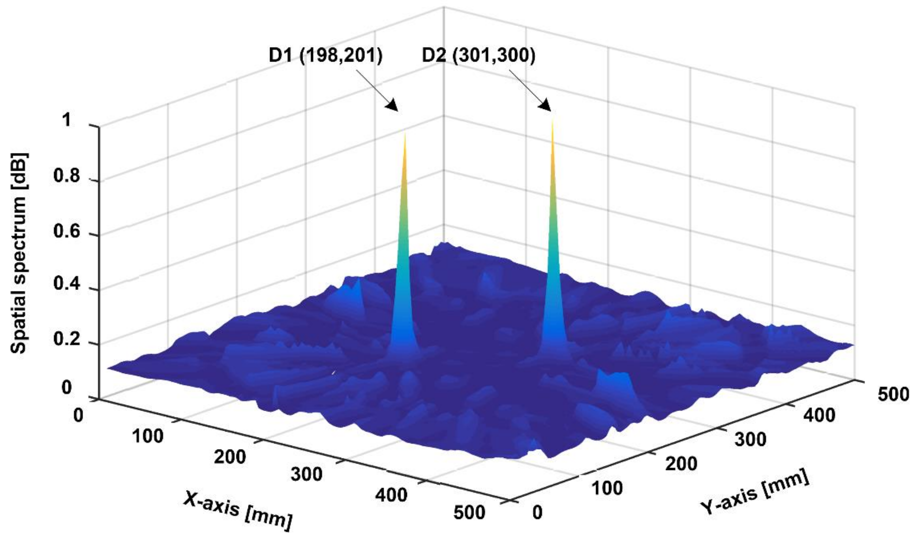

(a)

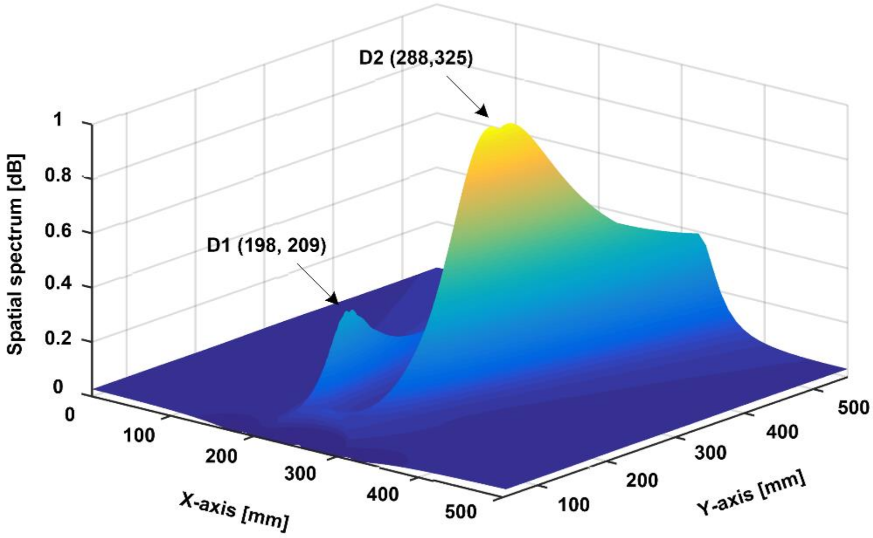

(b)

Fig. 6. Spatial spectra for C-II obtained by (a) Am-MUSIC algorithm; and (b) conventional MUSIC algorithm.

Provided that damage sites are in close proximity to each other – the case of C-III, the constructed spatial spectra using the Am-MUSIC method and conventional MUSIC method are compared in **Fig. 7**. In **Fig. 7(a)**, the two damage sites are localized precisely, in good agreement with the actual positions; however, only one damage site is identified by the conventional MUSIC algorithm with remarkable artifacts, in **Fig. 7(b)**, implying that the conventional MUSIC method may fail to detect multiple damage sites which are close one to another.

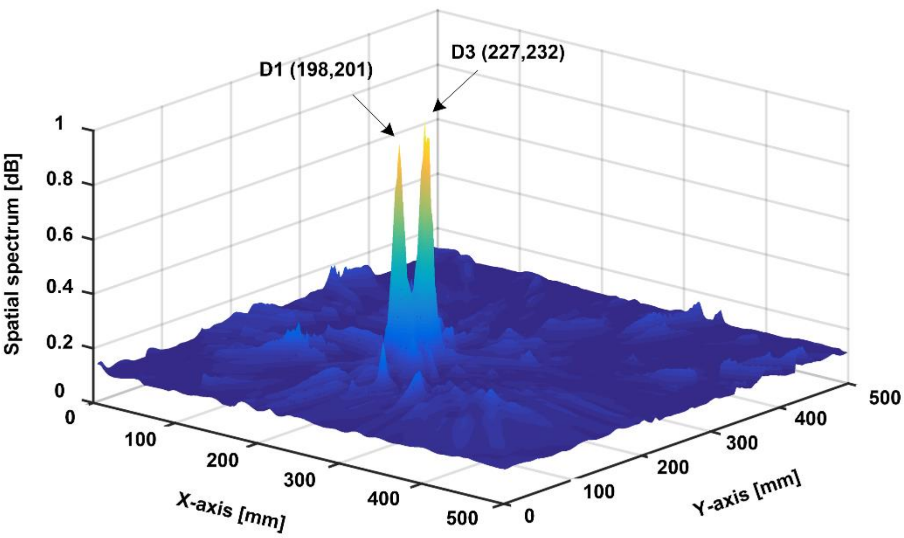

(a)

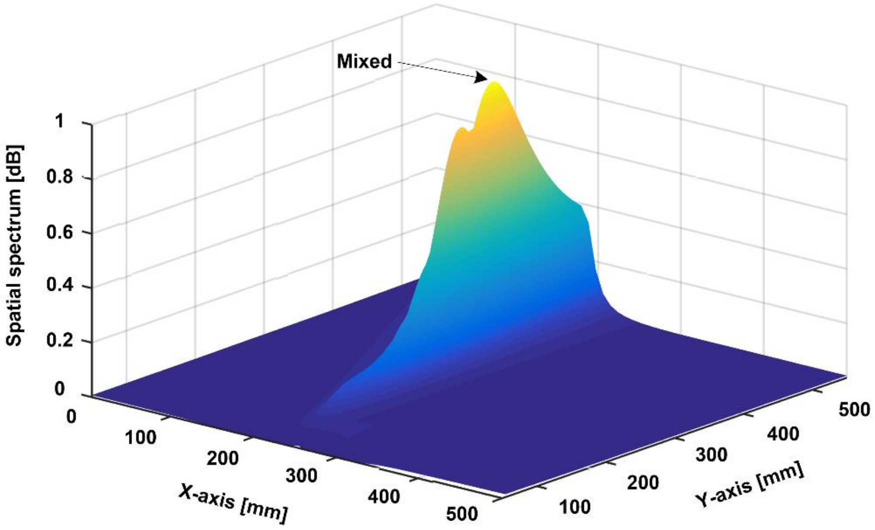

(b)

Fig. 7. Spatial spectra for C-III obtained by (a) Am-MUSIC algorithm; and (b) conventional MUSIC algorithm.

5. Experimental Validation

Subsequent to numerical simulation, effectiveness and accuracy of the Am-MUSIC-driven anomaly imaging is validated experimentally. A 2 mm-thick aluminum plate (dimensions: 1000 mm × 1000 mm × 2 mm; density: ρ=2700 kg/m^3; Young modulus: E=71 GPa; Poisson's ratio ν=0.33) is prepared. A sparse sensor network, consisting of eight PZT wafers (labelled as PZT-1, PZT-2, …, PZT-8), is surface-adhered on the plate, with the location of each wafer indicated in **Fig. 8(a)**. The experimental set-up is shown in **Fig. 8(b)**. The excitation signal – a Hanning-window-modulated 5-cycle toneburst at a central frequency of 200 kHz – is generated with an arbitrary waveform generator (NI® PXI-5412) and amplified by a linear power amplifier (Ciprian® US-TXP-3). The excitation signal is applied on each PZT wafer in turn to emit Lamb wave into the plate. S_0 mode Lamb wave signals, each in 300 μs, are acquired with a digital oscilloscope (NI® PXI-5105) at a sampling rate of 60 MHz.

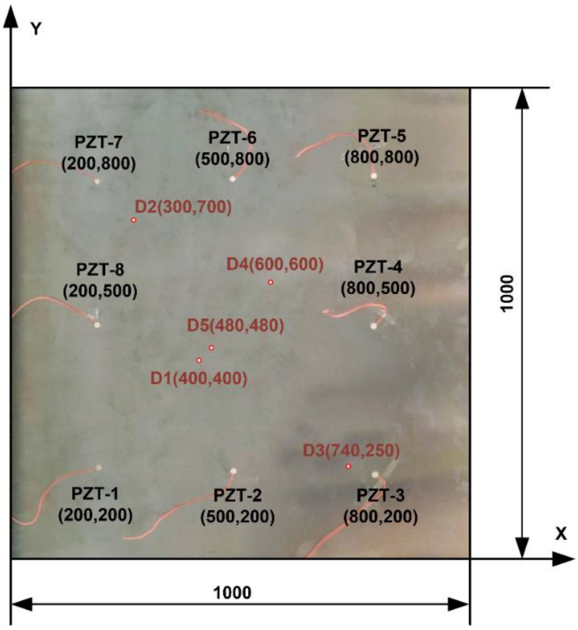

(a)

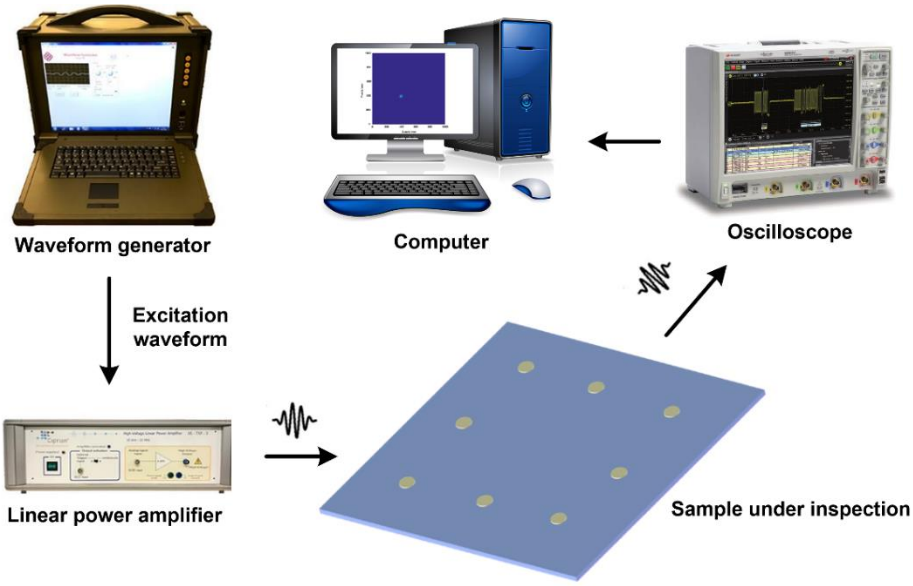

(b)

Fig. 8. (a) An aluminum plate with a surface-adhered sparse sensor network consisting of eight PZT wafers in experiment (red 'o': actual damage and all dimensions in mm); and (b) Experimental set-up.

Similar to the simulation in Section 4, three categories of damage are considered in the experiment, as recapped in **Table 3**.

Table 3 Damage cases in experiment

Damage Category	Damage Case	Damage
Single damage	E-I	A through-hole D1 at (400 mm, 400 mm)

		(Ø: 10 mm)
	E-II	A through-hole D2 at (300 mm, 700 mm) (Ø: 10 mm)
	E-III	A through-hole D3 at (740 mm, 250 mm) (Ø: 10 mm)
Double Damage (long distance apart)	E-IV	Two through-holes D1 at (400 mm, 400 mm) and D4 at (600 mm, 600 mm) respectively (Ø: 10 mm)
	E-V	Two through-holes D1 at (400 mm, 400 mm) and D2 at (300 mm, 700 mm) respectively (Ø: 10 mm)
Double Damage (short distance apart)	E-VI	Two through-holes D1 at (400 mm, 400 mm) and D5 at (480 mm, 480 mm) respectively (Ø: 10 mm)

The spatial spectra constructed using the Am-MUSIC algorithm for all the six damage cases are presented in **Fig. 9**, in which all damage sites are accurately located with precise depiction of the damage shape. In particular, for E-VI in which two damage sites are close one to the other, the algorithm still warrants high resolution and distinguishes individual damage sites.

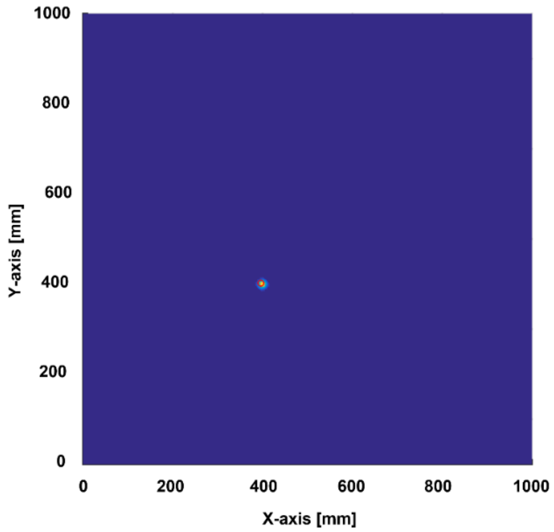

(a)

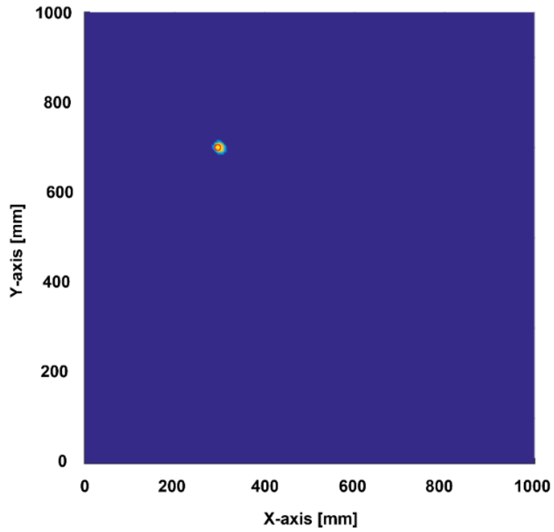

(b)

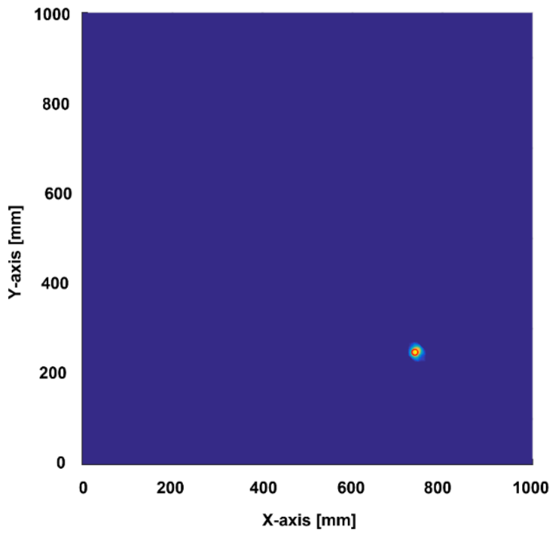

(c)

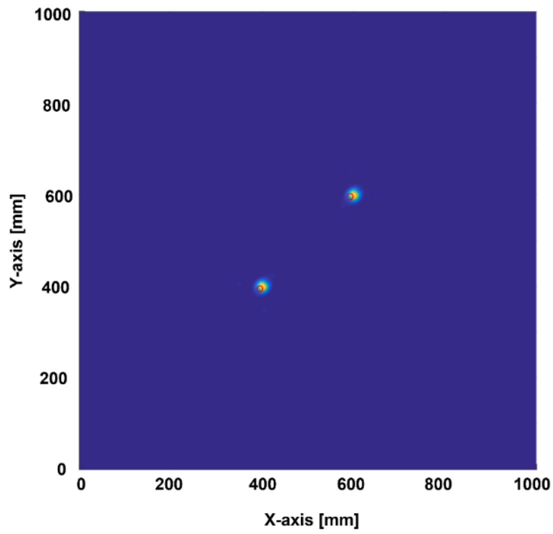

(d)

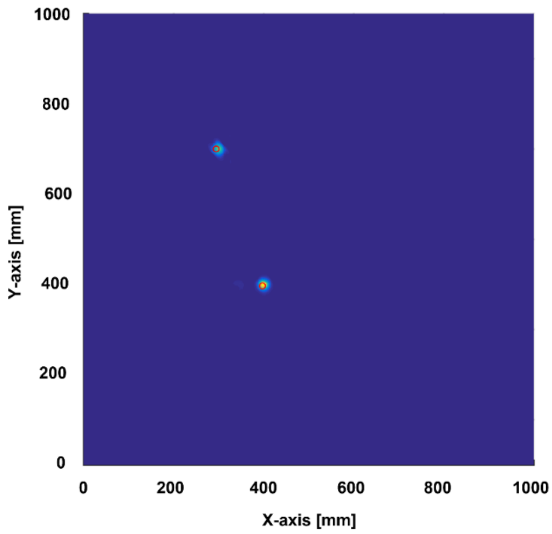

(e)

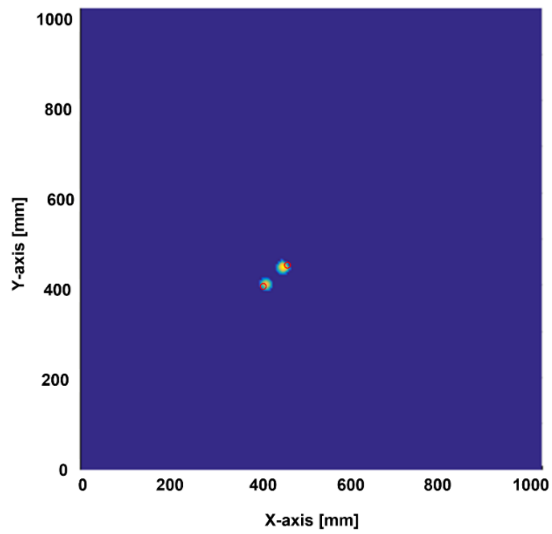

(f)

Fig. 9. Spatial spectra constructed using Am-MUSIC algorithm for damage case (a) E-I; (b) E-II; (c) E-III; (d) E-IV; (e) E-V; and (f) E-VI (red ‘o’: actual damage).

To take a step further, conventional MUSIC algorithm in junction with the use of a linear array is recalled for comparison. Seven PZT wafers are configured in a linear array as receivers, in **Fig. 10**, along with an additional PZT wafer as a wave actuator placed at the position (500 mm, 800 mm). Four typical damage cases (E-I, E-III, E-IV, E-VI) are analysed. The spatial spectra constructed using the conventional MUSIC algorithm are shown in **Fig. 11**, showing inferior accuracy in damage localization and sizing; moreover, it fails to differentiate multiple damage sites in E-VI that are close one from the other, and also fails to identify damage D3 in E-III that is located in the blind zone for a conventional MUSIC algorithm.

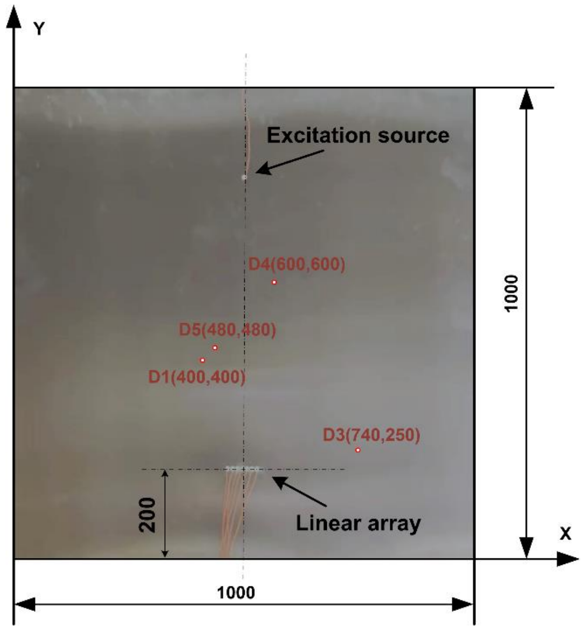

Fig. 10. An aluminum plate with a surface-adhered linear array consisting of 7 PZT wafers in experiment (red ‘o’: actual damage and all dimensions in mm).

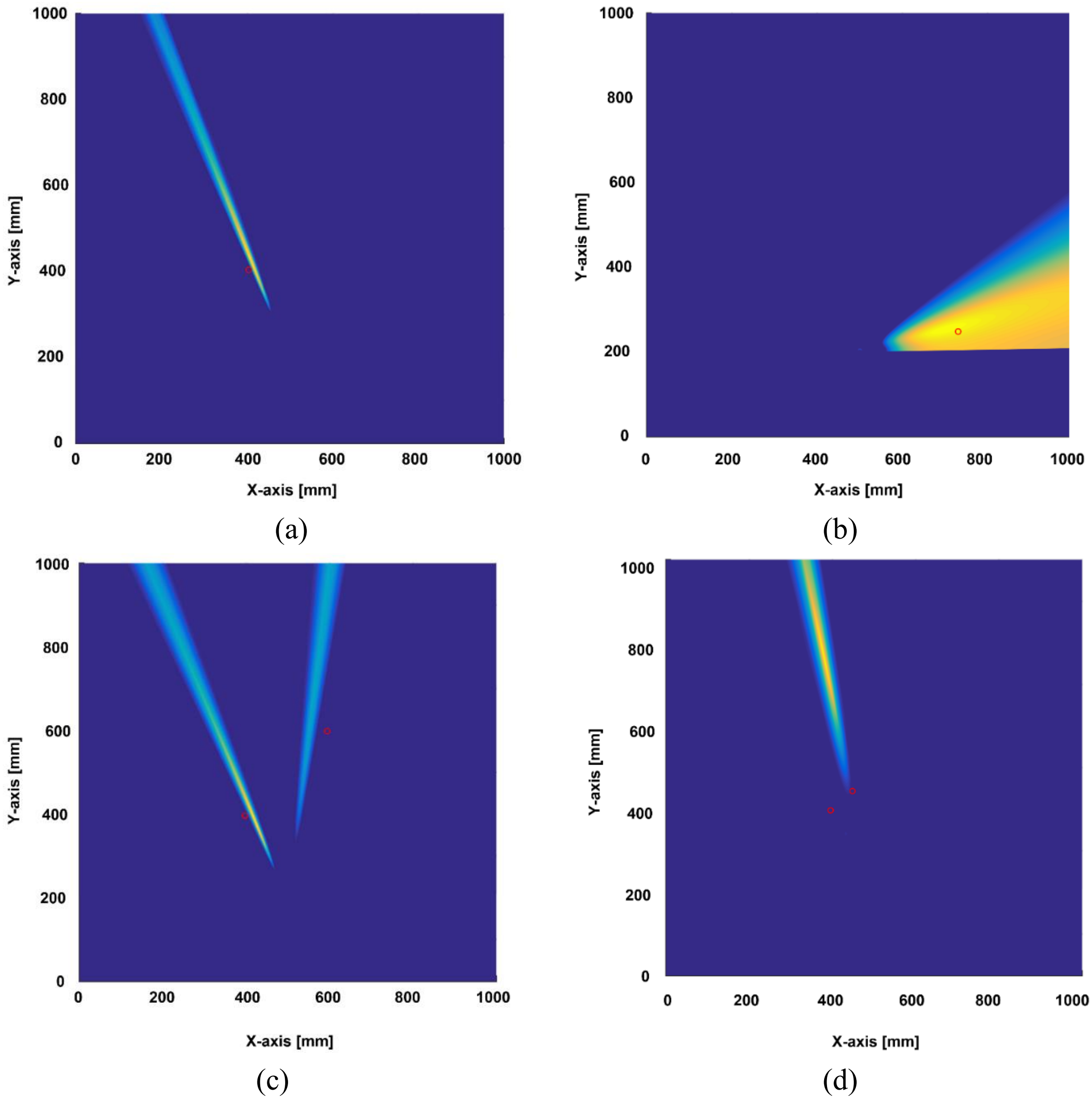

Fig. 11. Spatial spectra constructed using conventional MUSIC algorithm for damage case (a) E-I; (b) E-III; (c) E-IV; and (d) E-VI (red 'o': actual damage).

6. Concluding Remarks

Aimed to circumvent some critical limitations of the conventional MUSIC algorithm-based damage imaging, an ameliorated MUSIC algorithm is developed. In the Am-MUSIC algorithm, the signal representation matrix at each pixel is manipulated by the excitation signal series, instead of the scattered signal series, which enables the use of a sparse sensor network with arbitrarily positioned transducers rather than a linear array featuring a dense configuration of transducing elements with a uniform element pitch. By quantifying the orthogonal attributes between the signal subspace and noise subspace inherent in the signal representation matrix, a full spatial spectrum of the inspected sample can be generated, to visualize damage in the sample, irrespective of the damage quantity. The effectiveness and accuracy of the Am-MUSIC algorithm are verified in both simulation and experiment. Results show that compared with the conventional MUSIC methods, the Am-MUSIC algorithm is capable of improving the detectability (in particular for imaging of multiple damage sites that are close one to another) and eliminating blind zones. The Am-MUSIC is conducive to expanding conventional MUSIC from phased array-facilitated nondestructive evaluation to *in situ* health monitoring using built-in sparse sensor networks.

Acknowledgments

The work was supported by a General Project (No. 51875492) and a Key Project (No. 51635008) received from the National Natural Science Foundation of China. Z Su acknowledges the support from the Hong Kong Research Grants Council via General Research Funds (Nos. 15202820, 15204419 and 15212417).

References

[1] A.K.S. Jardine, D. Lin, D. Banjevic, A review on machinery diagnostics and prognostics implementing condition-based maintenance, Mechanical Systems and Signal Processing, 20 (2006) 1483-1510.
[2] Z. Su, L. Ye, Identification of damage using Lamb waves: from fundamentals to applications, Springer Science & Business Media, 2009.
[3] W. Ostachowicz, P. Kudela, P. Malinowski, T. Wandowski, Damage localisation in plate-like structures based on PZT sensors, Mechanical Systems and Signal Processing, 23 (2009) 1805-1829.

[4] L. Zeng, J. Lin, Structural damage imaging approaches based on Lamb waves: A review, 2011 International Conference on Quality, Reliability, Risk, Maintenance, and Safety Engineering, IEEE, 2011, pp. 986-993.
[5] P. Kudela, M. Radzienski, W. Ostachowicz, Z. Yang, Structural Health Monitoring system based on a concept of Lamb wave focusing by the piezoelectric array, Mechanical Systems and Signal Processing, 108 (2018) 21-32.
[6] H. Gao, Y. Shi, J.L. Rose, Guided wave tomography on an aircraft wing with leave in place sensors, AIP Conference Proceedings, American Institute of Physics, 2005, pp. 1788-1794.
[7] J.E. Michaels, Detection, localization and characterization of damage in plates with an in situ array of spatially distributed ultrasonic sensors, Smart Materials and Structures, 17 (2008) 035035.
[8] L. Qiu, S. Yuan, X. Zhang, Y. Wang, A time reversal focusing based impact imaging method and its evaluation on complex composite structures, Smart Materials and Structures, 20 (2011) 105014.
[9] C. Zhou, Z. Su, L. Cheng, Quantitative evaluation of orientation-specific damage using elastic waves and probability-based diagnostic imaging, Mechanical Systems and Signal Processing, 25 (2011) 2135-2156.
[10] S.-J. Wei, X.-L. Zhang, J. Shi, G. Xiang, Sparse reconstruction for SAR imaging based on compressed sensing, Progress In Electromagnetics Research, 109 (2010) 63-81.
[11] J.S. Hall, J.E. Michaels, Minimum variance ultrasonic imaging applied to an in situ sparse guided wave array, IEEE transactions on ultrasonics, ferroelectrics, and frequency control, 57 (2010) 2311-2323.
[12] M. Viberg, B. Ottersten, Sensor array processing based on subspace fitting, IEEE Transactions on signal processing, 39 (1991) 1110-1121.
[13] A.J. Hartemink, D.K. Gifford, T.S. Jaakkola, R.A. Young, Maximum-likelihood estimation of optimal scaling factors for expression array normalization, Microarrays: Optical technologies and informatics, International Society for Optics and Photonics, 2001, pp. 132-140.
[14] R. Schmidt, Multiple emitter location and signal parameter estimation, IEEE transactions on antennas and propagation, 34 (1986) 276-280.
[15] R.O. Schmidt, A signal subspace approach to multiple emitter location and spectral estimation, (1982).
[16] R. Compton, Two-dimensional imaging of radar targets with the MUSIC algorithm, 1987.
[17] T. Iwata, Y. Goto, H. Susaki, Application of the multiple signal classification (MUSIC) method for one-pulse burst-echo Doppler sonar data, Measurement Science and Technology, 12 (2001) 2178.
[18] P. Goldstein, R.J. Archuleta, Array analysis of seismic signals, Geophysical Research Letters, 14 (1987) 13-16.
[19] J.C. Mosher, S. Baillet, R.M. Leahy, EEG source localization and imaging using multiple signal classification approaches, Journal of Clinical Neurophysiology, 16 (1999) 225-238.
[20] M. Engholm, T. Stepinski, Direction of arrival estimation of Lamb waves using circular arrays, Structural Health Monitoring, 10 (2011) 467-480.
[21] H. Yang, T.J. Shin, S. Lee, Source location in plates based on the multiple sensors array method and wavelet analysis, Journal of Mechanical Science and Technology, 28 (2014) 1-8.
[22] H. Yang, Y.J. Lee, S.K. Lee, Impact source localization in plate utilizing multiple signal classification, Proceedings of the Institution of Mechanical Engineers, Part C: Journal of Mechanical Engineering Science, 227 (2013) 703-713.
[23] Y. Zhong, S. Yuan, L. Qiu, Multiple damage detection on aircraft composite structures using near-field MUSIC algorithm, Sensors and Actuators A: Physical, 214 (2014) 234-244.
[24] Y. Zhong, S. Yuan, L. Qiu, An improved two-dimensional multiple signal classification approach for impact localization on a composite structure, Structural Health Monitoring, 14 (2015) 385-401.

[25] S. Yuan, Q. Bao, L. Qiu, Y. Zhong, A single frequency component-based re-estimated MUSIC algorithm for impact localization on complex composite structures, Smart Materials and Structures, 24 (2015) 105021.
[26] H. Zuo, Z. Yang, C. Xu, S. Tian, X. Chen, Damage identification for plate-like structures using ultrasonic guided wave based on improved MUSIC method, Composite Structures, 203 (2018) 164-171.
[27] Q. Bao, S. Yuan, F. Guo, L. Qiu, Transmitter beamforming and weighted image fusion–based multiple signal classification algorithm for corrosion monitoring, Structural Health Monitoring, 18 (2019) 621-634.
[28] Q. Bao, S. Yuan, Y. Wang, L. Qiu, Anisotropy compensated MUSIC algorithm based composite structure damage imaging method, Composite Structures, 214 (2019) 293-303.
[29] V. Giurgiutiu, Structural health monitoring: with piezoelectric wafer active sensors, Elsevier, 2007.
[30] S. Sundararaman, D.E. Adams, E.J. Rigas, Structural damage identification in homogeneous and heterogeneous structures using beamforming, Structural Health Monitoring, 4 (2005) 171-190.
[31] A. Purekar, D. Pines, S. Sundararaman, D. Adams, Directional piezoelectric phased array filters for detecting damage in isotropic plates, Smart Materials and Structures, 13 (2004) 838.
[32] Y. Zhong, S. Yuan, L. Qiu, Multi-impact source localisation on aircraft composite structure using uniform linear PZT sensors array, Structure and Infrastructure Engineering, 11 (2015) 310-320.
[33] Y. Wang, K. Ho, Unified near-field and far-field localization for AOA and hybrid AOA-TDOA positionings, IEEE Transactions on Wireless Communications, 17 (2017) 1242-1254.
[34] E. Grosicki, K. Abed-Meraim, Y. Hua, A weighted linear prediction method for near-field source localization, IEEE Transactions on Signal Processing, 53 (2005) 3651-3660.
[35] A. Swindlehurst, T. Kailath, Passive direction-of-arrival and range estimation for near-field sources, IEEE Spec. Est. and Mod. Workshop, Citeseer, 1988.
[36] Q. Bao, S. Yuan, F. Guo, A new synthesis aperture-MUSIC algorithm for damage diagnosis on complex aircraft structures, Mechanical Systems and Signal Processing, 136 (2020) 106491.
[37] Y. Labyed, L. Huang, Ultrasound time-reversal MUSIC imaging with diffraction and attenuation compensation, IEEE transactions on ultrasonics, ferroelectrics, and frequency control, 59 (2012) 2186-2200.